Quadrotor Actuator Fault Diagnosis with Real-Time Experimental Results

Remus C Avram[1], Xiaodong Zhang[2] and Mohsen Khalili[3]

[1,2,3] *Wright State University, Dayton, Ohio, 45404, USA*
avram.3@wright.edu
xiaodong.zhang@wright.edu
khalili.4@wright.edu

ABSTRACT

Quadrotor Unmanned Aerial Vehicles (UAVs) have attracted significant attention in recent years due to their potentials in various military and commercial applications. Four propellers mounted on the shafts of four brushless DC motors generate the required thrust and torques needed for altitude and attitude control of quadrotors. However, structural damage to the propellers and rotor degradation can lead to actuator faults in the form of a partial loss of effectiveness in a rotor, which may result in degraded tracking performance or even loss of stability of the control system. This paper presents the systematic design, analysis, and real-time experimental results of a fault detection and isolation algorithm for quadrotor actuator faults using nonlinear adaptive estimation techniques. The fault diagnosis architecture consists of a nonlinear fault detection estimator and a bank of nonlinear adaptive fault isolation estimators designed based on the functional structures of the faults under consideration. Adaptive thresholds for fault detection and isolation are systematically designed to enhance the robustness and fault sensitivity of the diagnostic algorithm. Using an indoor quadrotor test environment, real-time experimental flight test results are shown to illustrate the effectiveness of the algorithms.

1. INTRODUCTION

In recent years, unmanned aerial vehicles (UAVs) have experienced a significant increase in popularity due to their potentials in various applications. Because of the requirement of autonomous operations without a human operator, autonomous navigation and control of UAVs are much more challenging. In order to enhance the reliability, survivability, and autonomy of UAVs, advanced health management technologies are required, which will enable UAVs to have the capabilities of state awareness and self-adaptation (Vachtsevanos, Tang, Drozeski, & Gutierrez, 2005; Y. M. Zhang et al., 2013; Shima & Rasmussen, 2009).

Quadrotors represent a special class of UAVs, which are equipped with four propellers, mounted on the shafts of four brushless DC motors, respectively. The spinning of the rotors generates the thrust required to maintain the quadrotor airborne. Additionally, the quadrotor attitude is controlled by systematically varying the rotor velocities which generate moment forces acting on the body frame. However, the actuating motor-propeller system is prone to faults due to component damage such as change in the motor parameters, propeller damage, etc. The occurrence of actuator faults can cause undesirable effects in the closed-loop control system that could lead to poor tracking performance and even catastrophic outcomes.

Recent research efforts guided towards quadrotor actuator faults focus mainly on the design of fault-tolerant control (FTC) systems, and systematic methods for actuator fault detection, isolation, and estimation (FDIE) are still limited (Y. M. Zhang et al., 2013; Chamseddine, Zhang, Rabbath, Apkarian, & Fulford, 2011; Z. T. Dydek, Annaswamy, & Lavretsky, 2013; Ranjbaran & Khorasani, 2010; Sharifi, Mirzaei, Gordon, & Zhang, 2010). Due to the intrinsic fabrication of the actuating systems, component damage can cause the faults to grow over time beyond the on-board FTC capabilities and reach actuator saturation. Therefore, early actuator fault detection and isolation plays a crucial role in the safe operation of quadrotor UAVs. Additionally, most actuator fault diagnosis methods with application to quadrotor UAVs are either based on linearization techniques or by assuming the quadrotor is operating in near hover conditions (Chamseddine et al., 2011; Ranjbaran & Khorasani, 2010; Sharifi et al., 2010). However, the quadrotor dynamics are highly nonlinear, and the assumption of near hover operating conditions is not always satisfied. Moreover, most of the existing results on quadrotor fault diagnosis designs focus on simulation studies, and experimental results are still very limited (Freddi, Longhi, & Monteri, 2010; Ranjbaran & Khorasani, 2010; Sharifi et al.,

2010; Berba, Lesecq, & Maritinez, 2008).

In this paper, a nonlinear framework for quadrotor actuator fault diagnosis is formulated based on the intrinsic nonlinearity of the system dynamics. A nonlinear adaptive estimation based method for detecting, isolating, and accommodating quadrotor actuator faults is developed by utilizing the general methodology in (X. Zhang, Polycarpou, & Parisini, 2002). The robustness and fault sensitivity properties of the fault detection and isolation algorithm is enhanced by using appropriately designed nonlinear adaptive thresholds. Additionally, the proposed actuator fault diagnosis method is independent of the on-board controller structure, and the fault magnitude estimate provided by the diagnostic component can be used to improve the overall performance of the closed-loop control system. The presented actuator fault diagnosis method is implemented using a real-time indoor quadrotor test environment. Experimental results are shown to illustrate the effectiveness of the diagnostic method.

The remainder of the paper is organized as follows. Section 2 presents the quadrotor dynamic model and formulates the problem of actuator fault diagnosis for quadrotor UAVs. Section 3 provides the detailed design of the fault detection, isolation, and estimation method. Real-time experiments from an in-door flight test environment are shown in Section 4, illustrating the effectiveness of the proposed method. Finally, some concluding remarks are given in Section 5.

2. PROBLEM FORMULATION

2.1. Quadrotor Dynamic Model

Figure 1 shows a simplified model of the quadrotor along with the assumed body frame orientation and Euler angles convention. Specifically, the quadrotor dynamics considered are described by:

$$\dot{p}_E = v_E \tag{1}$$

$$\dot{v}_E = \frac{1}{m} R_{EB}(\eta) \left(\begin{bmatrix} 0 \\ 0 \\ -U \end{bmatrix} - c_{\mathbf{d}} v_B \right) + \begin{bmatrix} 0 \\ 0 \\ g \end{bmatrix} + \xi_{v0}(x,t) + \xi_v(x,t) \tag{2}$$

$$\dot{\eta} = R_\eta(\phi,\theta)\omega \tag{3}$$

$$\dot{\omega} = \begin{bmatrix} \frac{J_y - J_z}{J_x} qr \\ \frac{J_z - J_x}{J_y} pr \\ \frac{J_x - J_y}{J_z} pq \end{bmatrix} + \begin{bmatrix} \frac{1}{J_x}\tau_\phi \\ \frac{1}{J_y}\tau_\theta \\ \frac{1}{J_z}\tau_\psi \end{bmatrix} + \xi_{\omega 0}(x,t) + \xi_\omega(x,t)\,, \tag{4}$$

where the system state variables are $p_E \in \mathbb{R}^3$, $v_E \in \mathbb{R}^3$, $\eta \triangleq [\phi, \theta, \psi]^T$, and $\omega \triangleq [p\,, q\,, r]^T$, representing the inertial position, inertial velocity, Euler angles, and body angular rates, respectively, and the system inputs include the thrust U, the rolling torque τ_ϕ, the pitching torque τ_θ, and the yawing torque τ_ψ. The rotation matrix R_{EB} in Eq. (2) is defined

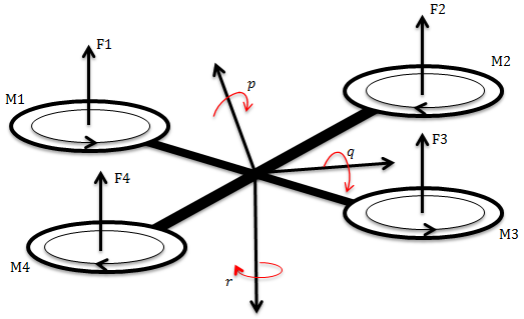

Figure 1. Quadrotor model in "X" configuration

based on a *3-2-1* rotation sequence as

$$R_{EB}(\eta) = \begin{bmatrix} c\theta c\psi & s\phi s\theta c\psi - c\phi s\psi & c\phi s\theta c\psi + s\phi s\psi \\ c\theta s\psi & s\phi s\theta s\psi + c\phi c\psi & c\phi s\theta s\psi - s\phi c\psi \\ -s\theta & s\phi c\theta & c\phi c\theta \end{bmatrix} \tag{5}$$

where $s\cdot$ and $c\cdot$ are shorthand notations for the $\sin(\cdot)$ and $\cos(\cdot)$ functions, respectively. Additionally, the matrix $R_\eta(\phi,\theta)$ in Eq. (3), relating body angular rates to Euler angle rates, is given by:

$$R_\eta(\phi,\theta) = \begin{bmatrix} 1 & \sin\phi\tan\theta & \cos\phi\tan\theta \\ 0 & \cos\phi & -\sin\phi \\ 0 & \sin\phi\sec\theta & \cos\phi\sec\theta \end{bmatrix}.$$

The term $c_{\mathbf{d}} v_B$ in Eq. (2) represents the drag force acting on the vehicle frame, with $c_{\mathbf{d}}$ being the drag force coefficient and v_B representing the velocity of the quadrotor relative to the body frame. The relationship between the inertial velocity v_E and the body velocity v_B is given by: $v_E = R_{EB} v_B$. The terms $\xi_{v0}(x,t)$ and $\xi_{\omega 0}(x,t)$ represent additional known nonlinearities (e.g. damping, gyroscopic effects, etc.) in the system dynamics, and $\xi_v(x,t)$ and $\xi_\omega(x,t)$ are the remaining modeling uncertainties in the translational and rotational dynamics, respectively, where $x \triangleq [p_E^T, v_E^T, \eta^T, \omega^T]^T$. Other model parameters in Eq. (1) - Eq. (4) are the quadrotor mass m, the gravitational acceleration g, and the quadrotor inertials about the body x-, y- and z-axis represented by J_x, J_y and J_z, respectively.

2.2. Actuator Fault Model

As shown in Figure 1, the motors and propellers are configured such that rotors $M1$ and $M3$ rotate counter-clockwise, and rotors $M2$ and $M4$ rotate clockwise. Each rotor is located at a distance d from the quadrotor center of mass and produces a force F_s ($s = 1, .., 4$) along the negative z direction relative to the body frame. Additionally, due to the spinning of the rotors, a reaction torque τ_s is generated on the quadrotor body by each rotor.

As in (Z. Dydek, Annaswamy, & Lavretsky, 2013; Amoozgar,

Chamseddine, & Zhang, 2013), we consider actuator faults represented by partial loss of effectiveness (LOE) in the rotors. For instance, structural damage to a propeller or an unexpected change in the rotor physical parameters would result in a partial loss of thrust generated by the respective rotor. Specifically, the actuator faults under consideration are modeled as follows: for $s = 1, .., 4$,

$$\Omega_s^* = \alpha_s \Omega_s \,, \tag{6}$$

where Ω_s represents the commanded rotor angular velocity, Ω_s^* is the actual rotor angular velocity, and $\alpha_s \in (\bar{\alpha}, 1]$ is an unknown parameter characterizing the occurrence of a partial loss of effectiveness fault in rotor s. The case of $\alpha_s = 1$ represents a healthy rotor, and $\alpha_s < 1$ represents a faulty rotor with partial loss of effectiveness. Note that the constant $\bar{\alpha} > 0$ is a known lower bound needed to maintain the controllability of the quadrotor. For instance, in the extreme case of a complete failure (i.e., $\bar{\alpha} = 0$), the quadrotor orientation becomes uncontrollable.

In this research, the thrust and torque generated by the rotors are considered to be directly proportional to the square velocity of the rotors (Pounds, Mahony, & Gresham, 2004; Y. M. Zhang et al., 2013). Specifically, by considering the actuator fault models Eq. (6), the relationship between the forces F_s and the reaction torques τ_s generated by each rotor and the rotor angular velocity is given by:

$$F_s = (1 - \beta(t - T_s)\vartheta_s) b_F {\Omega_s}^2 \tag{7}$$

$$\tau_s = -(1 - \beta(t - T_s)\vartheta_s) k \, \mathrm{sgn}(\Omega_s) {\Omega_s}^2 \,, \tag{8}$$

where $\vartheta_s \triangleq 1 - \alpha_s^2$ represents the unknown fault parameter relative to the the s-th rotor's square velocity. Specifically, $\vartheta_s = 0$ represents a healthy rotor, and $\vartheta_s \in (0, \bar{\vartheta})$ represents the case of a rotor experiencing a partial loss of effectiveness, where $\bar{\vartheta} \triangleq 1 - \bar{\alpha}^2$. The constants b_F and k represent rotor thrust and torque constants, respectively, and $\mathrm{sgn}(\cdot)$ represents the signum function. The fault time profile function $\beta(\cdot)$ is assumed to be a step function with unknown fault time occurrence T_s, that is:

$$\beta_s(t - T_s) = \begin{cases} 0 \,, & \text{if } t < T_s \\ 1 \,, & \text{if } t \geq T_s \,, \end{cases} \tag{9}$$

for $s = 1, .., 4$.

Thus, based on the quadrotor configuration shown in Figure 1 and by using Eq. (7)-Eq. (8), the total thrust and moments acting on the quadrotor body can be expressed as:

$$\begin{bmatrix} U \\ \tau_\phi \\ \tau_\theta \\ \tau_\psi \end{bmatrix} = M \left(I_4 - \beta(t - T_s)\vartheta_s \Lambda_s \right) \begin{bmatrix} \Omega_1^2 \\ \Omega_2^2 \\ \Omega_3^2 \\ \Omega_4^2 \end{bmatrix} \,, \tag{10}$$

where the vector $[\Omega_1^2, \, \Omega_2^2, \, \Omega_3^2, \, \Omega_4^2]^T$ represents the commanded rotor velocities, I_4 is the 4×4 identity matrix, and M represents the mapping matrix relating thrust and torques to rotor angular velocities (Pounds et al., 2004). Specifically, the mapping matrix is given by:

$$M = \begin{bmatrix} b_F & b_F & b_F & b_F \\ b_F a & -b_F a & -b_F a & b_F a \\ b_F a & b_F a & -b_F a & -b_F a \\ k & -k & k & -k \end{bmatrix} \,, \tag{11}$$

where $a = d/\sqrt{2}$, and d is the distance from the center of mass of each rotor to the center of mass of the quadrotor. The actuator fault distribution matrix Λ_s characterizes the location of an actuator fault for $s = 1, .., 4$. Specifically, Λ_s is a 4×4 matrix with all entries zero, except for the s-th position on the main diagonal. For instance, if a loss of effectiveness fault occurs in rotor $M1$, then $\Lambda_1 = \mathrm{diag}\{1, 0, 0, 0\}$.

In this brief, we consider the occurrence of a single actuator fault at any time. The research objective focuses on the design and experimental demonstration of a robust fault detection, isolation, and estimation scheme for quadrotor actuator faults described by Eq. (1)-Eq. (4) and Eq. (10) using adaptive estimation techniques. The following assumption is needed for the design and analysis of the FDI scheme:

Assumption 1: The unstructured modeling uncertainties $\xi_v(x, t)$ and $\xi_\omega(x, t)$ in Eq. (2) and Eq. (4), respectively, are unknown but assumed to be bounded by some known functions, i.e.,

$$|\xi_v(x, t)| \leq \bar{\xi}_v(x, t) \tag{12}$$

$$|\xi_\omega(x, t)| \leq \bar{\xi}_\omega(x, t) \tag{13}$$

for all $t \geq 0$.

Assumption 1 characterizes the class of modeling uncertainties under consideration. The bounds on the unstructured modeling uncertainties are needed in order to be able to derive adaptive thresholds to distinguish between the effects of faults and modeling uncertainty in the fault diagnosis procedure.

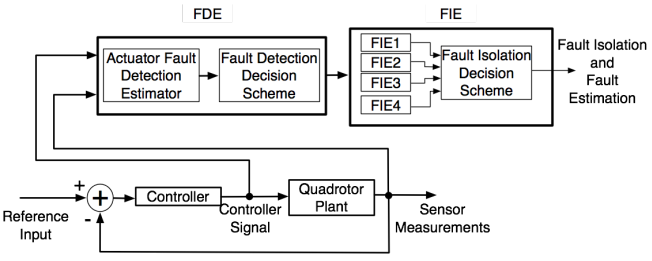

Figure 2. Quadrotor actuator fault diagnosis architecture

3. ACTUATOR FAULT DIAGNOSIS

The proposed actuator fault diagnosis and accommodation architecture is shown in Figure 2. As can be seen, it consists of

the following two main components: (1) a *fault detection estimator* (FDE) for determining fault occurrence and (2) a bank of four nonlinear adaptive *fault isolation estimators* (FIEs) for identifying the faulty rotor and providing an estimation of the unknown fault parameter. The controller signal and sensor measurements serve as inputs to the fault diagnosis module. Under normal operating conditions, the FDE monitors the system for detecting any faulty behaviors. Once an actuator fault is detected, the four FIEs are activated to isolate the faulty rotor and provide an estimate of the fault parameter. The robustness and fault sensitivity properties of the scheme are enhanced by the use of appropriately designed adaptive thresholds for fault detection and isolation.

3.1. Fault Detection

By substituting the thrust and torque model Eq. (10) into the quadrotor velocity and angular rate dynamics model given by Eq. (2) and Eq. (4), we obtain:

$$\begin{bmatrix} \dot{v}_z \\ \dot{p} \\ \dot{q} \\ \dot{r} \end{bmatrix} = \varphi(x,t) + GM(I_4 - \beta_s \vartheta_s \Lambda_s) \begin{bmatrix} \Omega_1^2 \\ \Omega_2^2 \\ \Omega_3^2 \\ \Omega_4^2 \end{bmatrix} + \xi(x,t), \quad (14)$$

where v_z represents the quadrotor inertial velocity along the $z-$direction (i.e. v_z is the third component of v_E), $G \triangleq \text{diag}\{-\frac{1}{m}\cos\phi\cos\theta,\ J_x^{-1},\ J_y^{-1},\ J_z^{-1}\}$, and the known nonlinearity $\varphi(x,t)$ is defined as:

$$\varphi(x,t) \triangleq \begin{bmatrix} -\frac{c_{\mathbf{d}}}{m} v_z + g \\ \frac{J_y - J_z}{J_x} qr \\ \frac{J_z - J_x}{J_y} pr \\ \frac{J_x - J_y}{J_z} pq \end{bmatrix} + \xi_0(x,t)\,. \quad (15)$$

The nonlinear terms $\xi_0(x,t)$ and $\xi(x,t)$ are given by:

$$\xi_0(x,t) \triangleq \begin{bmatrix} \xi_{z0}(x,t) \\ \xi_{\omega 0}(x,t) \end{bmatrix}, \quad \xi(x,t) \triangleq \begin{bmatrix} \xi_z(x,t) \\ \xi_\omega(x,t) \end{bmatrix}, \quad (16)$$

with $\xi_{z0}(x,t)$ and $\xi_z(x,t)$ being the third component of $\xi_{v0}(x,t)$ and $\xi_v(x,t)$ in Eq. (2), respectively. By using Eq. (14), the following nonlinear fault detection estimator is chosen:

$$\begin{bmatrix} \dot{\hat{v}}_z \\ \dot{\hat{p}} \\ \dot{\hat{q}} \\ \dot{\hat{r}} \end{bmatrix} = -L \begin{bmatrix} \hat{v}_z - v_z \\ \hat{p} - p \\ \hat{q} - q \\ \hat{r} - r \end{bmatrix} + \varphi(x,t) + GM \begin{bmatrix} \Omega_1^2 \\ \Omega_2^2 \\ \Omega_3^2 \\ \Omega_4^2 \end{bmatrix}, \quad (17)$$

where $[\hat{v}_z,\ \hat{p},\ \hat{q},\ \hat{r}]^T$ represents estimated inertial velocity and quadrotor angular rates, $L \triangleq \text{diag}\{l_j\}$, for $j = 1,..,4$, is a positive definite design matrix. Let us define the state estimation error as:

$$\begin{bmatrix} \tilde{v}_z \\ \tilde{p} \\ \tilde{q} \\ \tilde{r} \end{bmatrix} \triangleq \begin{bmatrix} v_z - \hat{v}_z \\ p - \hat{p} \\ q - \hat{q} \\ r - \hat{r} \end{bmatrix}, \quad (18)$$

and let $\varepsilon(t) \triangleq [\tilde{v}_z,\ \tilde{p},\ \tilde{q},\ \tilde{r}]^T$. Then, based on Eq. (14) and Eq. (17), it follows that the state estimation error dynamics are given by:

$$\dot{\varepsilon}(t) = -L\varepsilon(t) - GM\beta_s\vartheta_s\Lambda_s\bar{\Omega} + \xi(x,t)\,, \quad (19)$$

where

$$\bar{\Omega} \triangleq [\Omega_1^2,\ \Omega_2^2,\ \Omega_3^2,\ \Omega_4^2]^T\,. \quad (20)$$

Thus, in the absence of actuator faults (i.e., for $t_0 < T_s$), for $j = 1, \cdots, 4$, the j-th component of $\varepsilon(t)$ satisfies

$$|\varepsilon^j(t)| \le e^{-l_j(t-t_0)}|\varepsilon^j(t_0)| + \int_0^t \left| e^{-l_j(t-\tau)}\xi^j(x,\tau) \right| d\tau\,, \quad (21)$$

where $\varepsilon^j(t_0)$ is the initial state estimation error, and $\xi^j(x,t)$ is the j-th components of $\xi(x,t)$ given in Eq. (16). Based on Assumption 1, the modeling uncertainty $\xi^j(x,t)$ is bounded. Let us denote the bound on $\xi^j(x,t)$ as $\bar{\xi}^j(x,t)$ (i.e. $\bar{\xi}^j(x,t) \ge |\xi^j(x,t)|$). Therefore, based on Eq. (21), the fault detection thresholds can be chosen as

$$\bar{\varepsilon}^j(t) \triangleq e^{-l_j(t-t_0)}\bar{\varepsilon}^j(t_0) + \int_{t_0}^t e^{-l_j(t-\tau)}\bar{\xi}^j(x,\tau)d\tau\,, \quad (22)$$

where $\bar{\varepsilon}^j(t_0) \ge |\varepsilon^j(t_0)|$ is a bound on the initial state estimation error. Thus, it is guaranteed that $|\varepsilon^j(t)| \le \bar{\varepsilon}^j(t)$ for all $0 \le t < T_s$. Note that the adaptive detection thresholds described by Eq. (22) provide improved robustness and fault sensitivity over a fixed threshold (Blanke, Kinnaert, Lunze, & Staroswiecki, 2006; X. Zhang et al., 2002) and can be easily implemented as the output of the following linear filters:

$$\dot{\bar{\varepsilon}}^j(t) = -l_j\bar{\varepsilon}^j(t) + \bar{\xi}^j(x,t)\,. \quad (23)$$

with an initial condition $\bar{\varepsilon}^j(t_0)$.

Fault Detection Decision Scheme: If any component of the diagnostic residual $|\varepsilon^j(t)|$ exceeds its corresponding threshold $\bar{\varepsilon}^j(t)$ at some finite time $t^j > T_s$, then we can conclude that a fault has occurred. The fault detection time is defined as $T_d \triangleq \min\{t^j,\ j = 1,..,4\}$.

3.2. Fault Isolation

In this section, we describe the fault isolation method using adaptive estimation techniques. Suppose an actuator fault has occurred to the s-th actuator at time T_s, and the fault is detected at time $T_d > T_s$, where $s \in \{1,..,4\}$. Let us define the following state vector: $\zeta \triangleq [v_z, p, q, r]^T$. Therefore, based

on Eq. (14), for $t > T_d$, we have

$$\dot{\zeta} = f(\zeta, \bar{\Omega}) + \xi(x,t) + \vartheta_s h_s(x, \bar{\Omega}) \,, \tag{24}$$

where $\bar{\Omega}$ is defined in Eq. (20), $f(\zeta, \bar{\Omega}) \triangleq \varphi(x,t) + GM\bar{\Omega}$, and

$$h_s(x, \bar{\Omega}) \triangleq -GM\Lambda_s\bar{\Omega} \,, \tag{25}$$

is the known functional structure of the s-th actuator fault.

As shown in Figure 2, once an actuator fault is detected, a bank of four nonlinear adaptive FIEs are activated to determine the partially faulty rotor. Each FIE is designed based on the functional structure of a particular actuator fault under consideration. Specifically, by using Eq. (24), the following four FIEs are chosen: for $s = 1, \cdots, 4$,

$$\dot{\hat{\zeta}}_s \;\; = -\Gamma_s(\hat{\zeta}_s - \zeta) + f(\zeta, \bar{\Omega}) + \hat{\vartheta}_s h_s(x, \bar{\Omega}) \,, \tag{26}$$

where $\hat{\zeta}_s$ represents the state estimate, $\Gamma_s = \text{diag}\{\gamma_s^j\}$ is a positive definite design matrix ($j = 1, .., 4$), and $\hat{\vartheta}_s$ is the fault parameter estimate provided by the s-th FIE. The adaptation in the isolation estimators arises due to the unknown fault parameter ϑ_s. The adaptive law for estimating the unknown parameters $\hat{\vartheta}_s$ is derived using Lyapunov synthesis method (Ioannou & Sun, 1996) and is chosen as

$$\dot{\hat{\vartheta}}_s = \mathcal{P}_\Theta\{\Psi_s h_s^T(x, \bar{\Omega})(\zeta - \hat{\zeta}_s)\} \,, \tag{27}$$

where $\Psi_s > 0$ is a design constant representing the learning rate, and the projection operator $\mathcal{P}_\Theta$ is used to constrain the parameter estimate $\hat{\vartheta}_s$ to a known compact region $\Theta \triangleq [0,\, \bar{\vartheta}]$, ensuring the stability of the learning algorithm in the presence of modeling uncertainty (Ioannou & Sun, 1996).

Denote $\tilde{\zeta}_s$ as the state estimation error (i.e., $\tilde{\zeta}_s \triangleq \zeta - \hat{\zeta}_s$) corresponding to the s-th isolation estimator. Then, based on Eq. (24) and Eq. (26), for $t > T_d$, the dynamics of the j-th component of the state estimation error (i.e., $\tilde{\zeta}_s^j(t)$) is given by:

$$\dot{\tilde{\zeta}}_s^j = -\gamma_s^j \tilde{\zeta}_s^j + \vartheta_s h_s^j(x, \bar{\Omega}) - \hat{\vartheta}_s h_s^j(x, \bar{\Omega}) + \xi^j(x,t) \,. \tag{28}$$

The solution of the above differential equation satisfies

$$|\tilde{\zeta}_s^j| \le \int_{T_d}^{t} e^{-\gamma_s^j(t-\tau)} \left(|\vartheta - \hat{\vartheta}_s| \cdot |h_s^j(x, \bar{\Omega})| + |\xi^j(x,\tau)| \right) d\tau + e^{-\gamma_s^j(t-\tau)} \bar{\zeta}_s^j \,, \tag{29}$$

where the constant $\bar{\zeta}_s^j \ge |\tilde{\zeta}_s^j(T_d)|$ is an upper bound on the initial state estimation error. Since the parameter estimate $\hat{\vartheta}_s$ belongs to a known compact set Θ, we have $|\vartheta - \hat{\vartheta}_s| \le \kappa_s(t)$ for a suitable $\kappa_s(t)$ depending on the geometric properties of the set Θ. For instance, by choosing $\Theta \triangleq [0,\, \bar{\vartheta}]$, we have $\kappa_s(t) = \frac{\bar{\vartheta}}{2} + |\hat{\vartheta}_s - \frac{\bar{\vartheta}}{2}|$. Thus, by using Eq. (29) and Assumption 1, it can be shown $|\tilde{\zeta}_s^j(t)| \le \mu_s^j(t)$ for $t > T_d$, where

$$\mu_s^j(t) \triangleq \int_{T_d}^{t} e^{-\gamma_s^j(t-\tau)} \left[\kappa_s(\tau) |h_s^j(x, \bar{\Omega})| + \bar{\xi}^j(x,\tau) \right] d\tau + e^{-\gamma_s^j(t-\tau)} \bar{\zeta}_s^j \,. \tag{30}$$

Note that the adaptive threshold $\mu_s^j(t)$ given by Eq. (30) can easily be implemented as the outputs of a linear filter given by:

$$\dot{\mu}_s^j = -\gamma_s^j \mu_s^j + \kappa_s(t) |h_s^j(x, \bar{\Omega})| + \bar{\xi}^j(x,t) \,, \tag{31}$$

with an initial condition $\bar{\zeta}_s^j$.

The fault isolation procedure is designed based on the generalized observer scheme (Blanke et al., 2006). Specifically, the following intuitive principle is employed: if fault $s \in \{1, .., 4\}$ occurs at time T_s, and is detected at some finite time $T_d \ge T_s$, then a set of adaptive thresholds $\{\mu_s^j, j = 1, .., 4\}$ can be designed for the s-th FIE, such that all components of the state estimation error satisfy $|\tilde{\zeta}_s^j(t)| \le \mu_s^j(t)$ for all $t > T_d$. Consequently, a set of such adaptive thresholds can be designed for each of the four FIEs. In the fault isolation procedure, for a particular isolation estimator $r \in \{1, .., 4\} \backslash \{s\}$, if at least one component of its state estimation error exceeds the corresponding threshold, then the possibility of the occurrence of fault r can be excluded. Thus, we have the following:

Fault Isolation Decision Scheme: If, for each $r \in \{1, ..., 4\} \backslash \{s\}$, there exists some finite time $t_r > T_d$ and some $j \in \{1, .., 4\}$, such that $|\tilde{\zeta}_s^j(t_r)| > \mu_r^j(t_r)$, then the occurrence of a fault in the s-th actuator is concluded. The fault isolation time is defined as $T_{isol} \triangleq \max\{t_r,\, r \in \{1, .., 4\} \backslash \{s\}\}$.

3.3. Fault Estimation

After the faulty actuator is isolated, the matched adaptive FIE also provides an estimation of the unknown fault magnitude (see Eq. (27)). More specifically, after the occurrence of a fault corresponding to the s-th actuator, if there exists constants $\alpha_1 \ge \alpha_0 > 0$ and $T_0 > 0$, such that

$$\alpha_1 I \ge \frac{1}{T_0} \int_t^{t+T_0} h_s^T(x, \bar{\Omega}) h_s(x, \bar{\Omega}) d\tau \ge \alpha_0 I \,, \tag{32}$$

then the parameter estimate provided by the matched s-th FIE generated by Eq. (27) will closely approximate the true value of the fault parameter ϑ_s. Equation Eq. (32) provides the persistency of excitation (PE) condition which is typically required in many adaptive learning systems (Ioannou & Sun, 1996). It is worth noting that the unknown fault parameter ϑ_s in Eq. (24) is only a scalar and the required PE level can be easily satisfied.

Remark. An important feature of the presented integrated FDIE method is that it is independent of the baseline controller structure. As described above, the fault detection and isolation blocks shown in Figure 2 only use controller out-

put signals and sensor measurement in the fault detection, isolation, and estimation process. Therefore, the presented quadrotor FDIE method can possibly be deployed on-board of any quadrotor platform, provided that a good mathematical dynamics model and quadrotor physical parameters are available.

4. EXPERIMENTAL RESULTS

In this section, we present some real-time flight test results to illustrate the effectiveness of the proposed actuator fault detection, isolation, and estimation method.

4.1. Experimental Setup

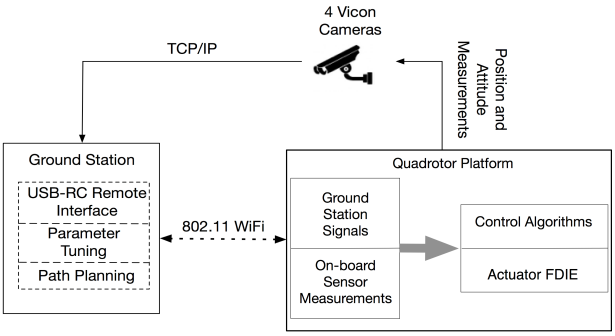

Figure 3. Experimental system architecture setup

A block diagram of the experimental system setup is shown in Figure 3. During flight tests, quadrotor position and attitude information is obtained from a Vicon motion capture camera system. The position and Euler angle measurements are collected every $10\,\mathrm{ms}$ and relayed from a Vicon dedicated PC via TCP/IP connection to a ground station computer with negligible time delay. The fault diagnosis method is implemented on-board of a quadrotor built in-house with off-the-shelf components, and it is evaluated in real-time during autonomous flight. The quadrotor is equipped with the Qbrain embedded control module from Quanser Inc. The control module consist of a HiQ acquisition card providing real-time IMU measurements, and a Gumstix DuoVero microcontroller running the real-time control software. An IEEE802.11 connection between the ground station PC and the Gumstix allows for fast and reliable wireless data transmission and on-line parameter tuning. The actuator fault diagnosis and FTC software executes on-board at $500\,\mathrm{Hz}$. In order to further take real-world constraints into account, the position and Euler angle measurements provided by the Vicon camera systems are intentionally corrupted by zero mean measurement noise. Note that in a real-world setting, position measurements can be obtained from a GPS unit. Additionally, an estimation of the roll, pitch, and yaw angles can be obtained using on-board sensor measurements (see for instance (John L. Crassidis, 2007)).

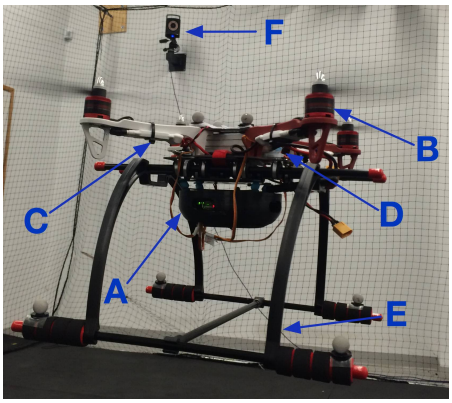

Figure 4. Experimental quadrotor platform in the Unmanned Air Vehicles Laboratory at Wright State University, Dayton OH.

Figure 4 shows the quadrotor while in flight, labeling the main components: Qbrain embedded control module (A), 4 propeller attached to four brushless DC motors mounted on a custom frame (B), four electronic speed controllers (C) regulating the rotors angular velocity based on the PWM signals generated by the on-board controller, a 3-cell 2000mAh, 12V battery (D), and a safety landing gear (E) added to provide improved protection of the control module during landing. Additionally, one of the Vicon cameras (F) can also be seen in the background.

Based on Eq. (1), the relationship between the quadrotor inertial velocity and the quadrotor altitude is given by $\dot{z}_E = v_z$, where z_E represents the quadrotor inertial vertical position. Then, using the fast rate position measurements, an estimate of the quadrotor inertial velocity can be obtained by means of linear filtering techniques. Specifically, the velocity v_z used in the FDI scheme is obtained as the output of the following second order filter:

$$v_z = \frac{\omega_0^2 s}{s^2 + 2\omega_0 s + \omega_0^2} z, \tag{33}$$

where z represents the altitude measurement, and ω_0 represents the corner frequency of the filter. For implementation purpose, the above filter is discretized and the corner frequency ω_0 is chosen experimentally to be $\omega_0 = 20\, rad/sec$.

The FDIE algorithm described in Section III is based on the quadrotor vertical velocity and angular rate dynamics (see Eq. (14)). It is worth noting that some of the modeling parameters in Eq. (14) are directly measurable or can be obtained experimentally (e.g. mass, moments of inertia, etc.). Conversely, motor thrust coefficients (b_F), the drag force coefficient ($c_{\mathbf{D}}$), and the additional known nonlinearities represented by the term $\xi_0(x,t)$ are not directly measurable and need to be estimated using system identification techniques (Klein & Morelli, 2006). Figure 5 shows the actual vertical velocity and angular rate dynamics and their estimates.

Specifically, referring to Eq. (14), the signals $\dot{v}_z$, $\dot{p}$, $\dot{q}$, and $\dot{r}$ generated using sensor measurements are depicted in dashed blue line, and their estimates generated based on the model given by the right side of Eq. (14) are depicted in solid red line. As can be seen, the model-based estimates closely approximate the actual signals.

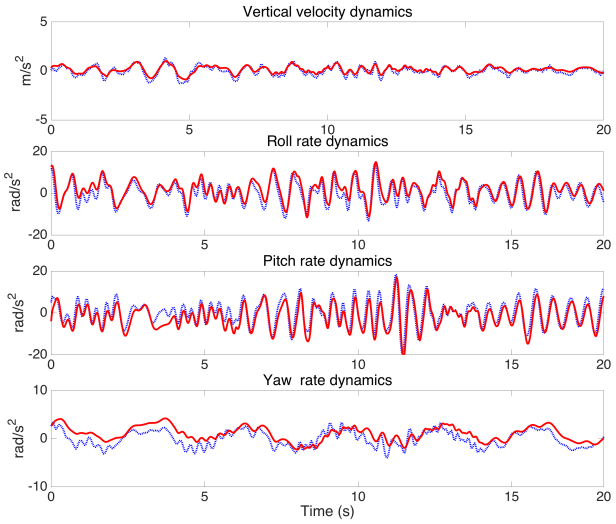

Figure 5. Quadrotor model system identification

The uncertainty bound $\bar{\xi}$ on the uncertainty term $\xi(x,t)$ given in Eq. (16) and Assumption 1 is obtained as follows. By using equation Eq. (24) under healthy actuator conditions (i.e. $\vartheta_s = 0$), we have

$$\xi(x,t) = \dot{\zeta} - f(\zeta,\bar{\Omega}) \leq \epsilon|\dot{\zeta} - f(\zeta,\bar{\Omega})| = \bar{\xi}(x,t,\bar{\Omega}), \quad (34)$$

where $\epsilon > 1$ is a constant chosen experimentally ($\epsilon = 1.25$ used in the results shown below). Specifically, the bound $\bar{\xi}$ is generated by using experimental data collected from several autonomous flight scenarios and standard system identification techniques using least squares (Klein & Morelli, 2006).

4.2. Experimental Evaluation Results

In order to evaluate the proposed actuator fault diagnosis method, approximately 1 minute of autonomous flight with real-time FDIE is recorded. The quadrotor is commanded to perform a circular maneuver with a radius of 1 meter at a constant altitude while following a sinusoidal orientation angle. Trajectory control of the quadrotor is achieved using a double-loop architecture, as shown in Figure 6. Specifically, the outer loop controls the x and y positions by generating desired roll and pitch angles. The *Altitude and Attitude Controller* generates the required rotor velocities needed for the quadrotor to track the desired attitude and altitude trajectories. As described above, the fault diagnosis method is independent of the structure of the controller. Therefore, for brevity, the description of the baseline control algorithms is purposely omitted.

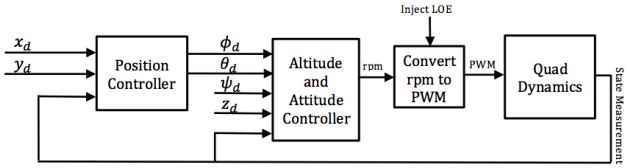

Figure 6. Quadrotor control architecture

Quadrotor sensor measurements are processed on-line, and real-time actuator fault diagnostic decision is provided by the diagnostic algorithm. An actuator fault is artificially injected in rotor $M1$ by purposely corrupting the controller output signal $\bar{\Omega}_1$ according to Eq. (6). Specifically, at approximately time $t = 24s$, a 20% loss of effectiveness is introduced in the thrust generated by rotor $M1$ (i.e. $\vartheta_1 = 0.20$, $\alpha_1 = 0.89$).

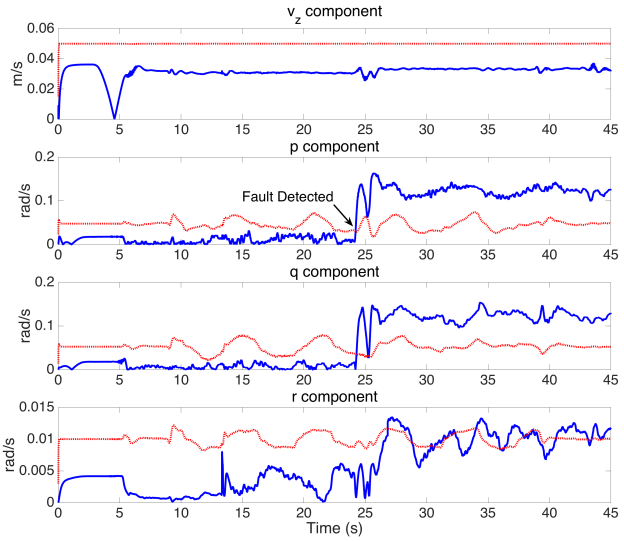

Figure 7. Fault detection results: detection residuals (solid blue lines) and adaptive thresholds (dashed red lines).

The fault detection residuals and adaptive thresholds, generated by Eq. (18) and Eq. (23), are shown in Figure 7. As can be seen, before the occurrence of an actuator fault, all components of the detection residuals remain below their corresponding thresholds. Shortly after the occurrence of a loss of effectiveness fault in rotor $M1$ at time $t = 24\,\text{sec}$, at least one residual component exceeds its corresponding detection threshold, indicating the occurrence of an actuator fault.

Figure 8 shows the isolation residuals and adaptive thresholds generated by the four FIEs, respectively. As can be seen, all components of the isolation residual generated by $FIE\,1$ always remain below their corresponding thresholds. Additionally, at least one component of the residual generated by any other FIEs exceeds the corresponding threshold shortly at approximately $t \approx 25\,\text{sec}$. Therefore, based on the fault

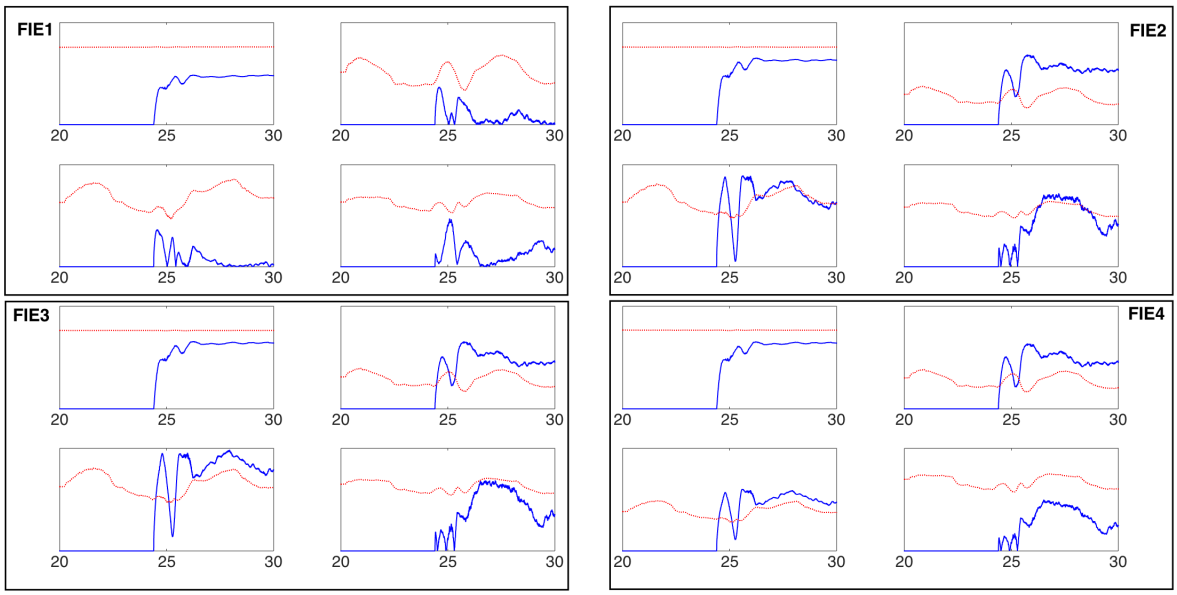

Figure 8. Fault isolation results: isolation residual components (solid blue lines) and adaptive thresholds (dashed red lines). The x-axis represents the time scale in seconds, and the y-axis units are m/s, rad/s, rad/s, rad/s starting with the top left plot of each FIE in a clockwise direction.

isolation logic described in Section 3.2, we can conclude that a fault has occurred in rotor $M1$.

As described in Section 3.2, the matched FIE provides a reasonable estimate of the fault magnitude. Figure 9 shows the estimated fault parameter generated by the adaptive law Eq. (27). As can be seen, shortly after fault detection (at approximately $t = 24.5\,\text{sec}$), the fault magnitude estimation reasonably approximates the true fault magnitude.

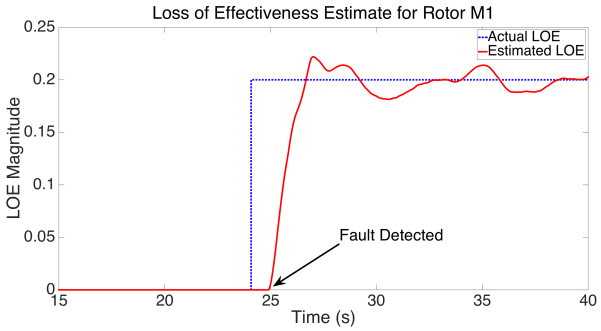

Figure 9. Fault parameter estimation

5. CONCLUSIONS

This paper presents the design and real-time experimental results of a quadrotor actuator fault diagnosis method using nonlinear adaptive estimation techniques. By following the general methodology given in (X. Zhang et al., 2002), a bank of nonlinear adaptive estimators are designed for detecting and isolating faults in the quadrotor actuating system. Nonlinear adaptive thresholds are designed to enhance the detectability and isolability of FDI method. The fault detection, isolation, and estimation method is implemented on a quadrotor UAV test environment and is demonstrated during real-time autonomous flight. An interesting direction for future research is to develop a unified FDI framework for both actuator faults and sensor faults in quadrotor UAVs.

REFERENCES

Amoozgar, M. H., Chamseddine, A., & Zhang, Y. M. (2013, August). Experimental test of a two-stage Kalman filter for actuator fault detection and diagnosis of an unmanned quadrotor helicopter. *Journal of Intelligent & Robotic Systems*, *70*(1), 107-117.

Berba, C., Lesecq, S., & Maritinez, J. (2008). A multi-observer switching strategy for fault-tolerant control of a quadrotor helicopter. In *16th Mediterranean Conference on Control and Automation* (p. 1094-1099).

Blanke, M., Kinnaert, M., Lunze, J., & Staroswiecki, M. (2006). *Diagnosis and Fault-Tolerant Control*. Berlin-Heidelberg: Springer.

Chamseddine, A., Zhang, Y., Rabbath, C.-A., Apkarian, J., & Fulford, C. (2011, 2016/08/11). Model reference adaptive fault tolerant control of a quadrotor uav. In *Infotech@aerospace 2011*. American Institute of Aeronautics and Astronautics.

Dydek, Z., Annaswamy, A., & Lavretsky, E. (2013, July). Adaptive control of quadrotor UAVs: A design trade study with flight evaluations. *IEEE Transactions on Control Systems Technology*, *21*(4), 1400-1406.

Dydek, Z. T., Annaswamy, A. M., & Lavretsky, E. (2013). Adaptive control of quadrotors UAVs: A design trade study with flight evaluations. *IEEE Transaction on Control Systems Technology*, *21*(4).

Freddi, A., Longhi, S., & Monteri, A. (2010, July). Actuator fault detection system for a mini-quadrotor. In *2010 IEEE International Symposium on Industrial Electronics* (p. 2055-2060).

Ioannou, P. A., & Sun, J. (1996). *Robust Adaptive Control*. Mineola, New York: Dover Publications, Inc.

John L. Crassidis, Y. C., F. Landis Markley. (2007). Survey of nonlinear attitude estimation methods. *Journal of Guidance, Control and Dynamics*, *30*(1).

Klein, V., & Morelli, E. A. (2006). *Aircraft system identification: Theory and practice* (1st ed.). American Institute of Aeronautics & Astronautics, Reston, VA.

Pounds, P., Mahony, R., & Gresham, J. (2004). Towards dynamically-favourable quad-rotor aerial robots. In *Australian Conference on Robotics and Automation, ACRA*.

Ranjbaran, M., & Khorasani, K. (2010, Dec). Fault recovery of an under-actuated quadrotor aerial vehicle. In *49th IEEE conference on Decision and Control (CDC)* (p. 4385-4392).

Sharifi, F., Mirzaei, M., Gordon, B., & Zhang, Y. (2010, Oct). Fault tolerant control of a quadrotor UAV using sliding mode control. In *2010 conference on control and Fault-Tolerant Systems (SysTol)* (p. 239-244).

Shima, T., & Rasmussen, S. (2009). *UAV cooperative decision and control* (T. Shima & S. Rasmussen, Eds.). Society for Industrial and Applied Mathematics. doi: 10.1137/1.9780898718584

Vachtsevanos, G., Tang, L., Drozeski, G., & Gutierrez, L. (2005). From mission planning to flight control of unmanned aerial vehicles: Strategies and implementation tools. *Anual Reviews in Control*, *29*, 101-115.

Zhang, X., Polycarpou, M., & Parisini, T. (2002, Apr). A robust detection and isolation scheme for abrupt and incipient faults in nonlinear systems. *IEEE Transactions on Automatic Control*, *47*(4), 576-593.

Zhang, Y. M., Chamseddine, A., Rabbath, C. A., Gordon, B. W., Su, C. Y., Rakheja, S., ... Gosselin, P. (2013, January). Development of advanced FDD and FTC techniques with application to an unmanned quadrotor helicopter testbed. *Journal of the Franklin Institue*, *350*(9).

BIOGRAPHIES

Remus C. Avram received his B.S. in Electrical Engineering with concentration in Computer Engineering at University of Texas, San Antonio, Texas in 2009. Remus obtained his M.S. and his Ph.D. in Electrical Engineering with concentration in Control Systems from Wright State University, Dayton, Ohio, in 2011 and 2016, respectively. Remus's main research include health diagnostic methods and advanced intelligent control.

Xiaodong Zhang received the B.S. degree from Huazhong University of Science and Technology, Wuhan, China, the M.S. degree from Shanghai Jiao Tong University, Shanghai, China, and the Ph.D. degree from University of Cincinnati, Cincinnati, OH, USA, all in electrical engineering, in 1994, 1997 and 2001, respectively. He is currently an Associate Professor of Electrical Engineering Department, Wright State University, Dayton, OH. His research interests include intelligent control systems, fault diagnosis and prognosis, fault-tolerant control, verification and validation of control systems for safety assurance, etc. He is an Associate Editor of the IEEE Transactions on Control Systems Technology and a member of the IFAC SAFEPROCESS Technical Committee.

Mohsen Khalili received the B.S. degree from Bahonar University of Kerman, Kerman, Iran, the M.S. degree from Sharif University of Technology, Tehran, Iran, both in electrical engineering, in 2007 and 2009, respectively. He is currently a Ph.D. Candidate in Electrical Engineering department at Wright State University, OH, USA. His research interests are fault diagnosis, prognosis, and fault-tolerant control of multi-agent systems.